Çankaya University Journal of Science and Engineering
Volume 14, No. 2 (2017) 134-151

Solid Oxide Fuel Cell Thermodynamic Study

Youcef Sahli[1,2,*], Bariza Zitouni[3], Hocine Ben-Moussa[1]

[1]*Department of Mechanical Engineering, Faculty of Technology. University of Batna 2, Algeria.*
[2]*Unité de Recherche en Energies Renouvelables en Milieu Saharien, URERMS, Centre de Développement des Energies Renouvelables, CDER 01000, Adrar, Algérie,*
[3]*Department of Food Technology. Institute of Veterinary Sciences and Agricultural Sciences. University of Batna 1, Algeria.*
e-mail: sahli.sofc@mail.com/y.sahli@urerms.dz, zitounibariza@yahoo.fr, h2sofc@gmail.com

Abstract: The aim of this work is the solid oxide fuel cell (SOFC) thermodynamic study. Particular attention is given to the electric power optimization. The Nernst potential and the over-potentials that are due to the concentration polarization, activation polarization and to the Ohm polarization represent the fuel cell potential. A FORTRAN language program was developed locally for the cell model simulation.

From the result analysis, it appears that the developed model allowed understanding the operating condition effects on both potential and power density values. The obtained results show that the cell potential and the power density are proportional to the operating temperature changes and to the oxygen concentration in the oxidant, by cons, they are inversely related to the supply pressure changes, fuel moisture and to the electrolyte thickness.

Keywords: SOFC, power density, over-potential, thermodynamic.

1. Introduction

Among the fuel cell types, solid electrolyte cell (SOFC) delivers a large electric power. It is considered as a promising technology for its great global performance and its operating ability by several fuels.

The electrochemical behavior remains the main research focus for the fuel cell development. The complexity and the multitude of phenomena involved in the fuel cell operation make its experimental study difficult. Thus, researchers incite to develop numerical simulation programs in order to predict better the phenomena behavior that intervenes and minimizes the costly experimental experiences. In this context, several studies have been addressed previously. Yang et al. [1] have developed an electrochemical model for solid oxide fuel cells to a supported anode (SOFC-AS) to analyze and improve the cell design. The presented model takes into

ISSN 2564 – 7954

account three over-potential types: activation, Ohm and concentration. They showed that the activation and Ohm over-potentials are the main responsible cause for the tension loss. Al Zahrani et al. [2] have presented and used a model for predicting the conventional SOFC performance under various operating conditions and design for low operating temperatures.

Verma et al. [3] have studied the possibility of supplying the solid oxide fuel cells with reformed fuels. This can be beneficial because they are cheap compared to pure hydrogen. A biomass fuel can be easily modeled as a reformed fuel because it can be converted into H_2 and CO using the gasification or the bio-degradation. This produced composition is mainly made in a gas reformer situated before the cell. Saebea et al. [4] have performed a study to evaluate the theoretical performance of a single cell of an SOFC integrated with a steam reforming process using three different renewable fuels: ethanol, glycerol and biogas. They studied the main operating parameter effects on the hydrogen production. Tippawan et al. [5] have applied a thermodynamic concept to identify a reforming process suitable for an SOFC supplied with ethanol. Three different reforming technologies are considered, specifically, steam reforming, partial and direct oxidation reforming. They showed the effects of the main operating parameters on the distribution of reforming products, such as (H_2, CO, CO_2 and CH_4) in order to identify the best process for reforming ethanol for SOFC applications.

This study is a continuation of our previous ones [6-15]. In [6], the thermoelectric performance of an intermediate temperature SOFC has been presented by a one-dimensional model for the parallel direction to the gas flow using the finite volume method. The heat is generated by the Joule's effect and the loss due to the internal chemical reaction. In the reference [11], the power density and the hydrogen consumption of a planar SOFC are studied according to input parameters; such as the operating temperature, the operating pressure, the flow rates and the mass fractions by a one-dimensional electro-dynamic model using the finite difference method.

In the reference [7], the hydrogen and water distribution depending on the anode thickness in the SOFC heart has been realized by a two-dimensional model based on the finite difference method in the perpendicular plane to the reactive gas flow directions. Reference [8] shows a two-dimensional numerical study of the temperature fields in the perpendicular plane to the gas flow of a planar SOFC heart at a supported anode under the chemical reactions effect.

The reference [9] represents a study of the location and determination of the maximum temperature values in all solid and porous parts (electrolyte, interconnectors, anode and cathode) of the planar SOFC at a supported anode or a supported electrolyte, in a perpendicular plane to the gas flow under the polarization effects: Ohmic, activation and concentration. Reference [10] shows an analysis of the heat production and distribution in all solid and porous

parts of the planar SOFC at a supported anode under the effect of various over-potentials (Ohmic, activation, concentration and chemical), in the perpendicular plane to the gas flow direction in order to describe the thermal behavior during the operation. The reference [12] represents a comparative study of the heat distribution depending on the gas supply temperature between two planar SOFC configuration types. The first has a supported anode and the second has a supported electrolyte for the cases with and without the total heat source (Ohmic, concentration, activation and chemical), in all solid and porous parts (electrolyte, interconnectors, anode and cathode) of the planar SOFC. In [13], the molar fractions effect of the fuel constitutive chemical species (CH_4, H_2O, CO, CO_2 and H_2) on the heat distribution is studied in a planar SOFC at the supported anode in a two-dimensional environment and perpendicular to the gas flow direction. Heat generation/absorption due to the direct internal reforming in all solid and porous parts of the cell are discussed. The reference [14] presents a study of the produced heat behavior by the direct internal reforming depending on the temperature and pressure of the supply fuel in all parts of the planar SOFC at a supported anode in the perpendicular plane to the gas flow.

In the reference [15], a comparative study of the heat generation in the three geometric configuration types of the planar SOFC (supported anode, supported cathode and supported electrolyte) in a three-dimensional environment is realized. The heat production is caused by the Joule's effect.

In this paper, an SOFC thermodynamic study is presented, while paying particular attention to optimize the produced power density by the fuel cell. Studied parameters are the operating temperature, the operating pressure, the water and oxygen concentrations and the electrolyte thickness.

2. Thermodynamic Modeling

2.1. Fuel Cell Performance

SOFC tension is defined by the difference between the theoretical Nernst potential and the sum of different generated tension losses by several phenomena:

$$E = E_{Nernst} - Tension\ losses \tag{1}$$

'E' (V) is the SOFC tension, 'E_{Nernst}' (V) is the Nernst potential that is given by the following equation:

$$E_{Nernst} = E_0 + \frac{R.T}{n.F}.\left[ln\left(\frac{P_{H_2}.P^{0.5}{}_{O_2}}{P_{H_2O}}\right)\right] \tag{2}$$

Where '*R*' (Kg.m^{-1}.s^{-1}) is the gas constant, '*T*' (K) is the operating temperature, '*n*' is the transfer electron number, '*F*' (C.mol^{-1}) is the Faraday number, '*P*' (bar) is the partial pressure of each species (hydrogen, oxygen and water steam) and 'E_0' (V) is the ideal potential. It is defined by a first order polynomial as a temperature function given in Equation (3). [16-24]:

$$E_0 = a + b.T \tag{3}$$

Where '*a*' (V) and '*b*' (V.K^{-1}) are constant, they are defined by the Table 1:

TABLE 1. Ideal potential coefficients; 'a' and 'b'.

a [V]	b [V.K^{-1}]	References
1,253	-2,4516.10^{-4}	[16-24]

The tension losses that are defined by equation (1) include three loss types; Ohmic, activation and concentration.

2.2. Ohm Losses

The Ohmic losses are due to the encountered resistance by the ionic current passing through the electrolyte and due to the encountered resistance by the electrons that traversed the electrodes and the electric circuit. They are mainly due to the electrolyte. They can be reduced by decreasing the electrolyte thickness and improving the ionic conductivity. However, the electrolyte and electrodes obey the Ohm's law. The Ohmic losses are defined by the Equation (4) [3,9,25-31]:

$$\eta_{Ohm} = i.r_j \tag{4}$$

Where '*i*' (A.m^{-2}) is the current density and '*r*' is the electrical resistance of each component '*j*' (anode, cathode and electrolyte), which is defined for each component by the ratio of the element thickness '*e*' (m) and his electrical conductivity 'σ' (Ω^{-1}.cm^{-1}) in equation (5). The electrical conductivity of each element is given by the standard materials ((YSZ) for the electrolyte, (LSM) for the cathode and (Ni-YSZ) for the anode)n as shown in Table 2.

$$r = \frac{e}{\sigma} \tag{5}$$

TABLE 2. The electrical conductivity of each component of the cell.

Components	σ [Ω^{-1}.cm^{-1}]	References
Electrolyte	$\sigma_{ele} = 3{,}34.10^4.e^{\left(\frac{-10300}{T}\right)}$	[3,9,15,25-31]
Cathode	$\sigma_{cat} = \frac{4{,}2.10^7}{T}.e^{\left(\frac{-1200}{T}\right)}$	[3,9,15,25-31]
Anode	$\sigma_{an} = \frac{9{,}5.10^7}{T}.e^{\left(\frac{-1150}{T}\right)}$	[3,9,15,25-31]

2.3. Activation Losses

The activation losses are present when the electrochemical reaction rate at the electrode surface is controlled by the deceleration kinetics for this electrode. In other words, the activation polarizations are directly related to the electrochemical reaction rate. In order that a chemical or electrochemical reaction can start in both cases, the reactants must exceed an activation barrier. In the electrochemical reaction case where the activation losses 'η_{act}' (V) exceed (50-100 mV), they are described by Equation (6). [5,17,18,21,23,32]:

$$\eta_{Act,j} = \frac{R.T}{\alpha.n.F}.\sinh^{-1}\left(\frac{i}{2.i_{0,j}}\right) \quad (6)$$

Where 'α' is the electronic transfer coefficient or the charge transfer coefficient and 'i_0' (A.m^{-2}) is the exchange current density for each electrode 'j' (anode or cathode), it is usually given by Equation (7) [5,17,18,21,23,32]:

$$i_{0,j} = k_j.\exp\left(-\frac{E_j}{R.T}\right) \quad (7)$$

Where 'E_j' (J.mol^{-1}) and 'k_j' (A.m^{-2}) are the pre-exponential factor and the activation energy of each electrode 'j' (anode and cathode), they are represented respectively by a first order polynomial as a temperature function and a constant (see Table 3).

TABLE 3. Values and expressions of the pre-exponential factor and the activation energy.

Anode		Cathode		References
k_{an}[A.m^{-2}]	E_{an}[J.mol^{-1}]	k_{cat} [A.m^{-2}]	E_{cat} [J.mol^{-1}]	
$6{,}54.10^{11}.\frac{R.T}{2.F}$	$1{,}4.10^{5}$	$2{,}35.10^{11}.\frac{R.T}{2.F}$	$1{,}37.10^{5}$	[5,17,18,21,23,32]

2.4. Concentration Losses

At the electrodes, the concentration losses are the potential losses due to the system inability to maintain the initial reactant concentrations. Many factors can contribute: the low gas diffusion through the porous electrodes, the reactant or product dissolution in the electrodes and the reactant or product diffusions in the reaction site. These losses may be expressed by the following simplified equation [33,34]:

$$\eta_{Conc,j} = -\frac{R.T}{n.F}.ln\left(1-\frac{i}{i_{l,j}}\right) \quad (8)$$

Where 'i_l' (A.m^{-2}) is the limiting current density of each electrode 'j' (anode and cathode) that are represented by constants (see Table 4).

TABLE 4. Limiting current density values for each electrode.

Anode [A.m^{-2}]	Cathode [A.m^{-2}]	References
$2{,}99.10^{4}$	$2{,}16.10^{4}$	[33,34]

2.5. Code Structure

After collecting the equations that represent the physical model, realization procedure of a calculator code in FORTRAN will begin. This code consists of four steps; the first step represents the data reading which consists of the following parameters: the ideal potential coefficients 'a' and 'b', the operating temperature 'T' and the supply pressure 'P', the concentrations of the three species 'X_{H2}', 'X_{H2O}' and 'X_{O2}', the limiting current density of each electrode '$i_{l,an}$' and '$i_{l,cat}$', the transfer electron number 'n', the Faraday number 'F' and the thickness of each cell heart component 'e_{an}', 'e_{cat}' and 'e_{ele}'. The second step concerns the variable calculations that are not current density functions: the ideal and Nernst potentials 'E_0' and 'E_{Nernst}', the electrical conductivities of the anode 'σ_{an}', the cathode 'σ_{cat}' and the electrolyte

'σ_{ele}', the electrical resistances of the electrolyte 'r_{ele}' and the electrodes 'r_{an}' and 'r_{cat}', the pre-exponential factors of the anode 'K_{an}' and the cathode 'K_{cat}' and the anode and cathode exchange current densities '$i_{0,an}$' and '$i_{0,cat}$'. The third step concerns the variable calculations that are current density functions which are: the activation, the concentration and the Ohmic losses of each component '$\eta_{act,an}$', '$\eta_{act,cat}$', '$\eta_{conc,an}$', '$\eta_{conc,an}$', '$\eta_{Ohm,an}$', '$\eta_{Ohm,cat}$' and '$\eta_{Ohm,ele}$', the cell tension 'E' and the cell power density 'P_d' for each current density value. Finally, the fourth step is the result display. The calculator code chart is given by the Figure 1.

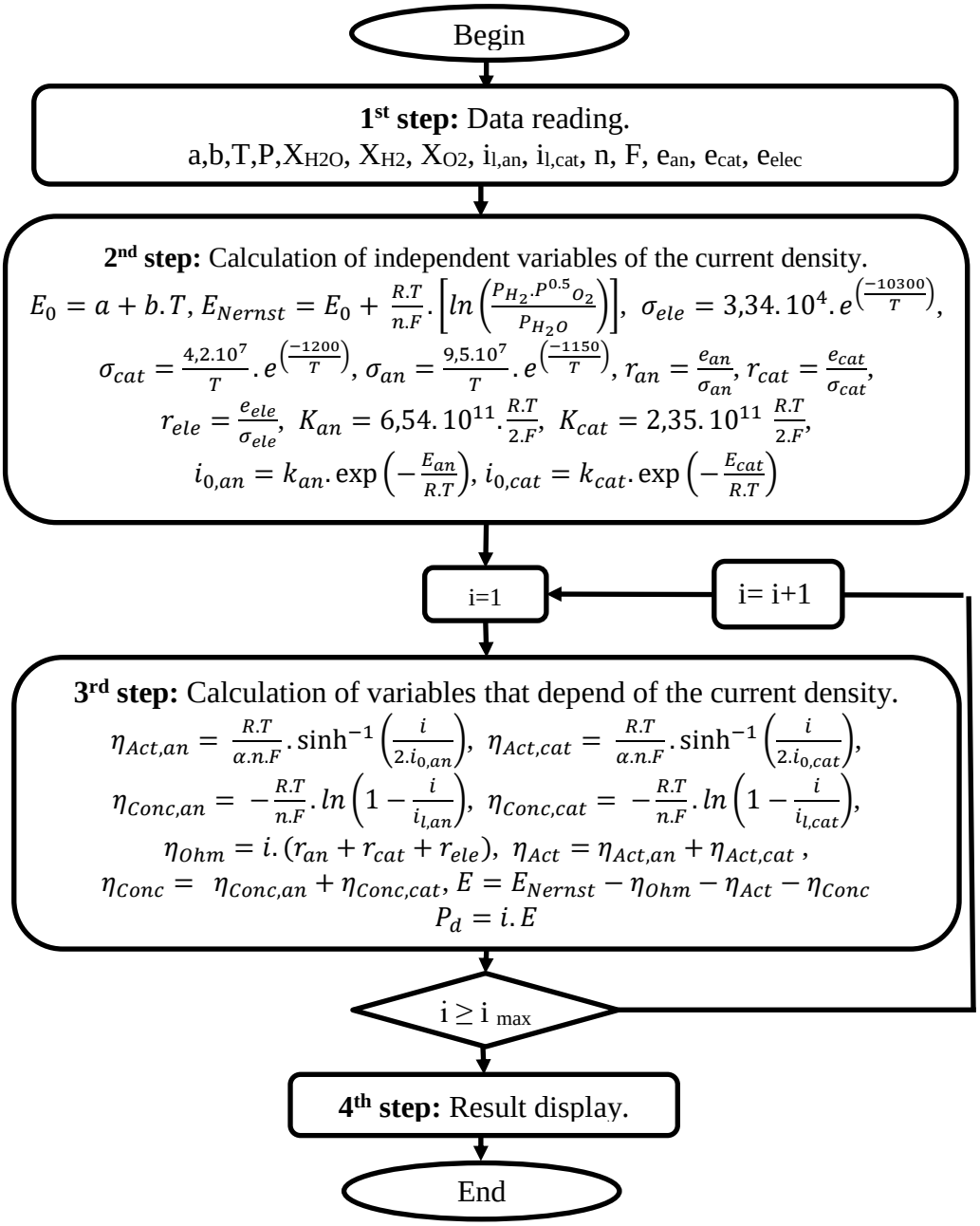

FIGURE 1. Resolution algorithm.

3. Results and Discussion

After writing a computer Fortran language program based on the previously presented model [3,5,9,16-32], all object curves in our study are made using a spreadsheet type visualization software to plot these obtained curves.

The results are presented in five classes. In the first class, the impact of each polarization on the total polarization is demonstrated. In the second class, the explanation of the operating temperature effect on the cell potential and power density is presented. While in the third class, the supply pressure effect on the potential and the power density is discussed. As to the fourth class, the water steam and oxygen concentration contributions in the variation of the cell potential and power density are illustrated. Finally, the fifth class concerns the obtained results analysis with the different electrolyte thickness dimensions. All parameter values that are used for obtaining these results are given in Table 5.

TABLE 5. Used parameter values in the simulation.

Parameters	Class 1	Class 2	Class 3	Class 4-a	Class 4-b	Class 5
T, (k)	1073	973,1073,1173	1073	1073	1073	1073
P, (bar)	1	1	1,2,3	1	1	1
X_{H2O}	0.05	0.05	0.05	0.03,0.06,0.09	0.05	0.05
X_{H2}	0.95	0.95	0.95	0.97,0.94,0.91	0.95	0.95
X_{O2}	0.21	0.21	0.21	0.21	0.21,0.5,1	0.21
e_{an}, (μm)	100	100	100	100	100	100
e_{cat}, (μm)	100	100	100	100	100	100
e_{ele}, (μm)	50	50	50	50	50	5,50,500

3.1. Impact of each Polarization on the Total Polarization

Polarization and power density curves are obtained in the case of a solid oxide fuel cell at supported electrodes. The electrolyte and electrodes are supposed to be made with standard materials: (Ni-YSZ) for the anode, (LSM) for the cathode and (YSZ) for the electrolyte. Cell heart element thicknesses are (100 μm) for the electrodes and (50μm) for the electrolyte. The cell is supplied with the humidified hydrogen as fuel (X_{H2O} = 0,05) and the air as an oxidizer

(X_{O2} = 0,21). Fuel and air pressure values are the same (1bar). The operating temperature is assumed to be the same and equal to (1073 K). Three distinct loss types are shown in Figure 2. The first is the greatest loss. It is generated by the Ohmic polarization and localized mainly at the electrolyte. The second potential drop is due to the activation over-potential. The third is the smallest loss; it brings up the reactive diffusion problem to the catalytic sites. In addition, the cell potential maximum value reached in this simulation is (0,7731 V). It is alone of Nernst to a nil current density.

The maximum current density is about (17000 $A.m^{-2}$) which is suitable for very low potential and very large exothermic. The maximum produced power density by the cell is upper to (3027 $W.m^{-2}$); it is defined by a current density of (8390 $A.m^{-2}$). In the minimum current density values, the power density is low. It increases hyperbolically in relation to the current density up to its maximum value at (8390 $A.m^{-2}$), then a hyperbolic collapse of the power density that is resulted by the different over-potentials.

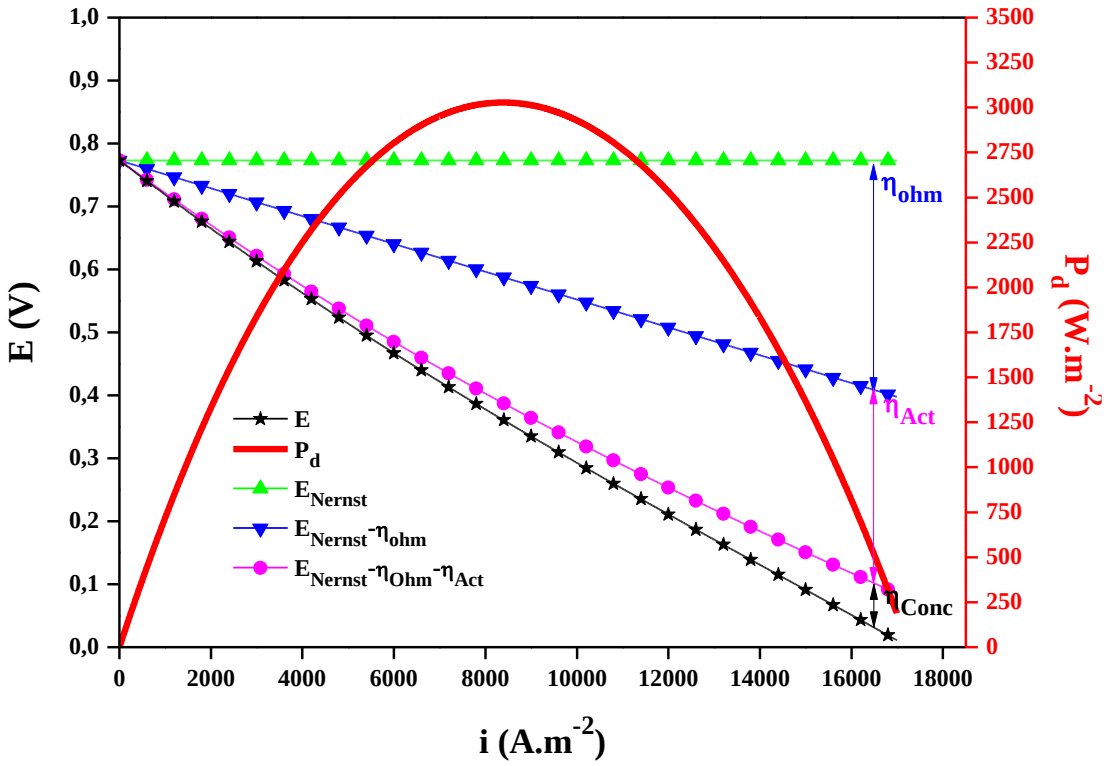

FIGURE 2. SOFC tension, power density and all over-potentials curves.

3.2. Operating Temperature Influence

The operating temperature effect on the polarization and the power density values is shown in Figure 3. The fuel is the humidified hydrogen (X_{H2O} = 0,05), and the air is the oxidant (X_{O2} = 0,21). Supply pressure is common for the fuel and the air. It is identical to one bar. The operating temperatures are supposed similar to (973, 1073 and 1173 K). In addition, the important Nernst potential noticed among the three carried out tests is the one which suits with an operating temperature equal to (973 K). The minor Nernst potential value is recorded for an operating temperature identical to (1173 K). Reasonably, the Nernst potential that corresponds to an operating temperature similar to (1073 K) is between the two Nernst potentials previously exposed. The highest values of the real potential and the power density belong to the cell operating at a temperature similar to (1173 K). The lowest values of the power density and the real potential are recorded for the cell operating at a temperature equivalent to (973 K). However, an operating temperature of (1073 K) leads to power density and real potential average values, which demonstrates that the Nernst potential is inversely proportional to the cell operating temperature. Hence, the real potential is proportional to the cell operating temperature. In other words, all the losses are inversely proportional to the cell operating temperature, which leads directly to a potential and a power density proportional to the operating temperature.

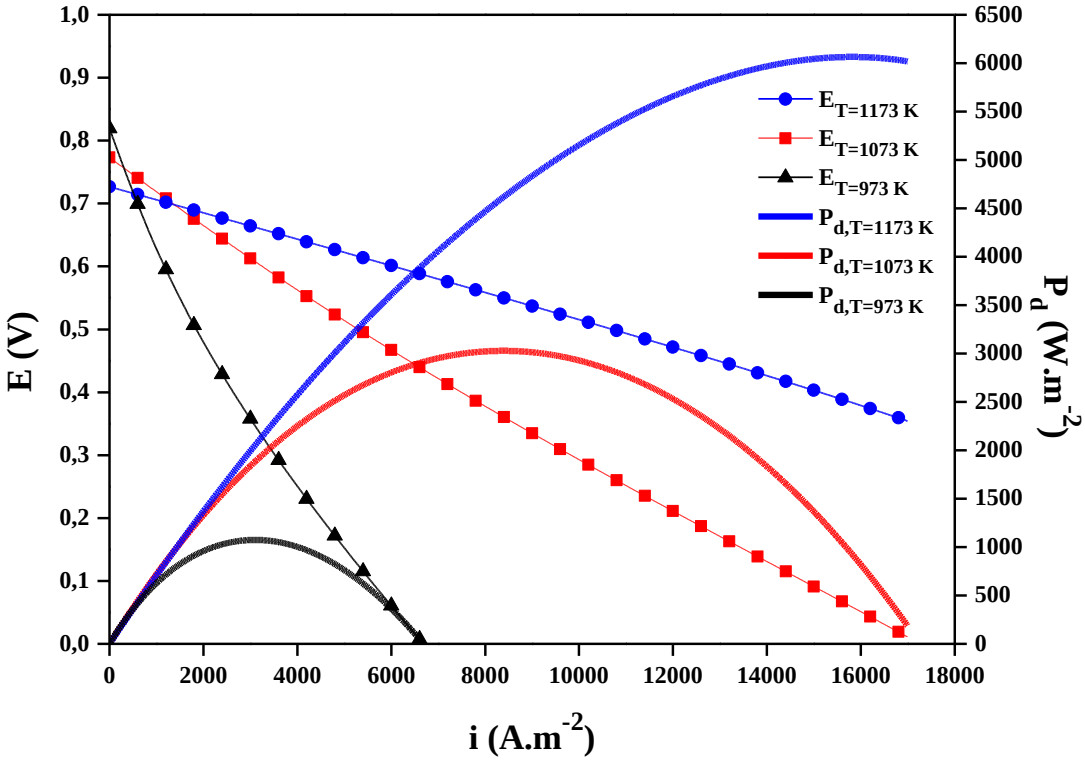

FIGURE 3. Potential and power density evolutions according to the operating temperature.

3.3. Supply Pressure Effect

The operating pressure effect on the polarization and power density curves, which are obtained by the model simulation, is shown in Figure 4. The supply pressures are common for both gasses; they are recognized by (1, 2 and 3 bars). In addition, the highest values of Nernst potential, real potential and power density noticed in the three tests belong to the cell having a supply pressure identical to one bar. While the lowest values of Nernst potential, real potential and power density recorded in the realized simulation tests belong to the cell that has a supply pressure of four bars. Logically, the Nernst potential, real potential and power density that correspond to an intermediate air and fuel supply pressure have intermediate values which are between the values of the two Nernst potentials, two real potentials and two power densities presented previously. It means that the Nernst potential and power density are inversely proportional to the cell operating pressure. It is because the change in the cell operating pressure does not influence all the over-potentials.

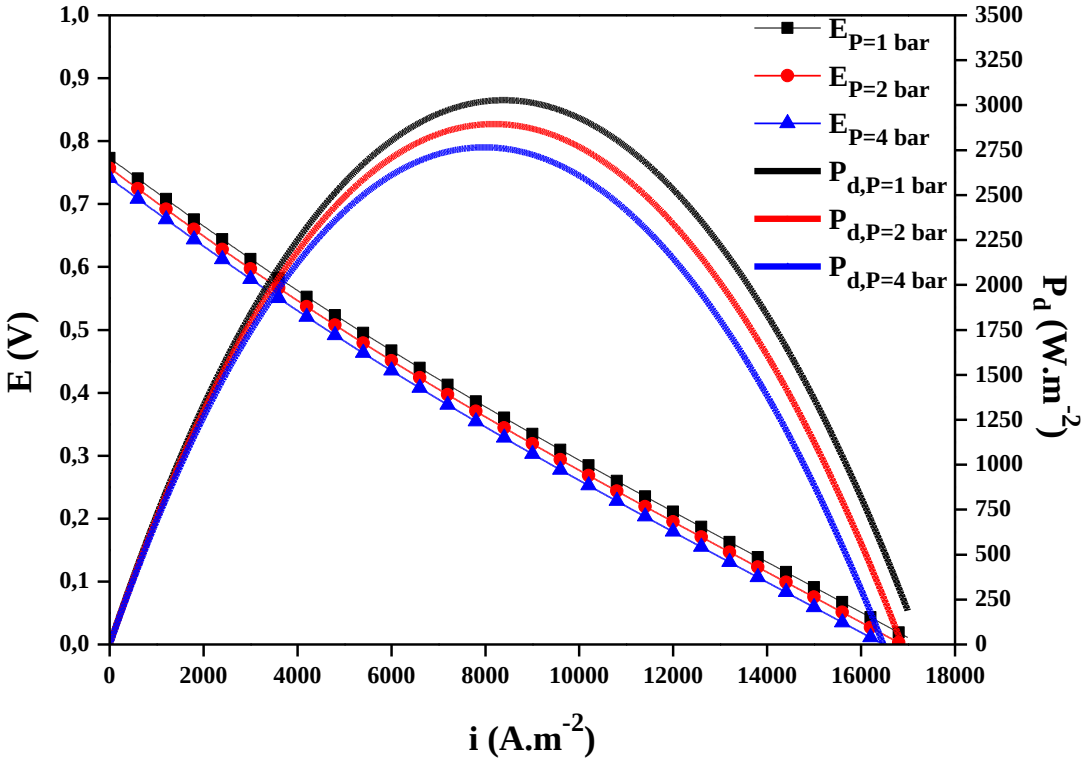

FIGURE 4. Potential and power density evolutions according to the operating pressure.

3.4. Steam and Oxygen Concentration Effects

Figure 5 shows the effect of the steam content in the fuel and the oxygen concentration in oxidant on the different polarizations and on the delivered cell power density.

The cell operating temperature is identical to (1073 K). Hydrogen humidification rates are (X_{H2O} = 0,03, 0,06 and 0,09). The oxygen concentration rates in the oxidizer are (X_{O2} = 0,21, 0,50 and 1,00). The highest values of Nernst potential, real potential and power density noticed in the performed tests on the various water contents are the values that fit a fuel humidity rate of (0,03). Whereas the smallest values of the same parameters are recorded for the cell that has a fuel humidification rate of (0,09). The Nernst potential, real potential and power density corresponding to a middle fuel humidification rate have average values that are between the two Nernst potentials, two real potentials and two power density cited previously. It means that the Nernst potential, real potential and power density are inversely proportional to the fuel humidification rate. For an SOFC cell that operates by the pure oxygen as oxidizer, the values of Nernst potential, real potential and power density are maximal. These parameters take minimal values for the air as an oxidizer of an oxygen rate of (0,21). Logically, the Nernst potential, real potential and power density correspond to an oxygen rate in the oxidizer of (0,50). They have intermediate values which are between the two Nernst potentials, two real potentials and two power densities discussed previously. The Nernst potential and real potential are proportional to the oxygen concentration rate in the oxidant. In addition, the cell power density is proportional to the oxygen concentration in the oxidant.

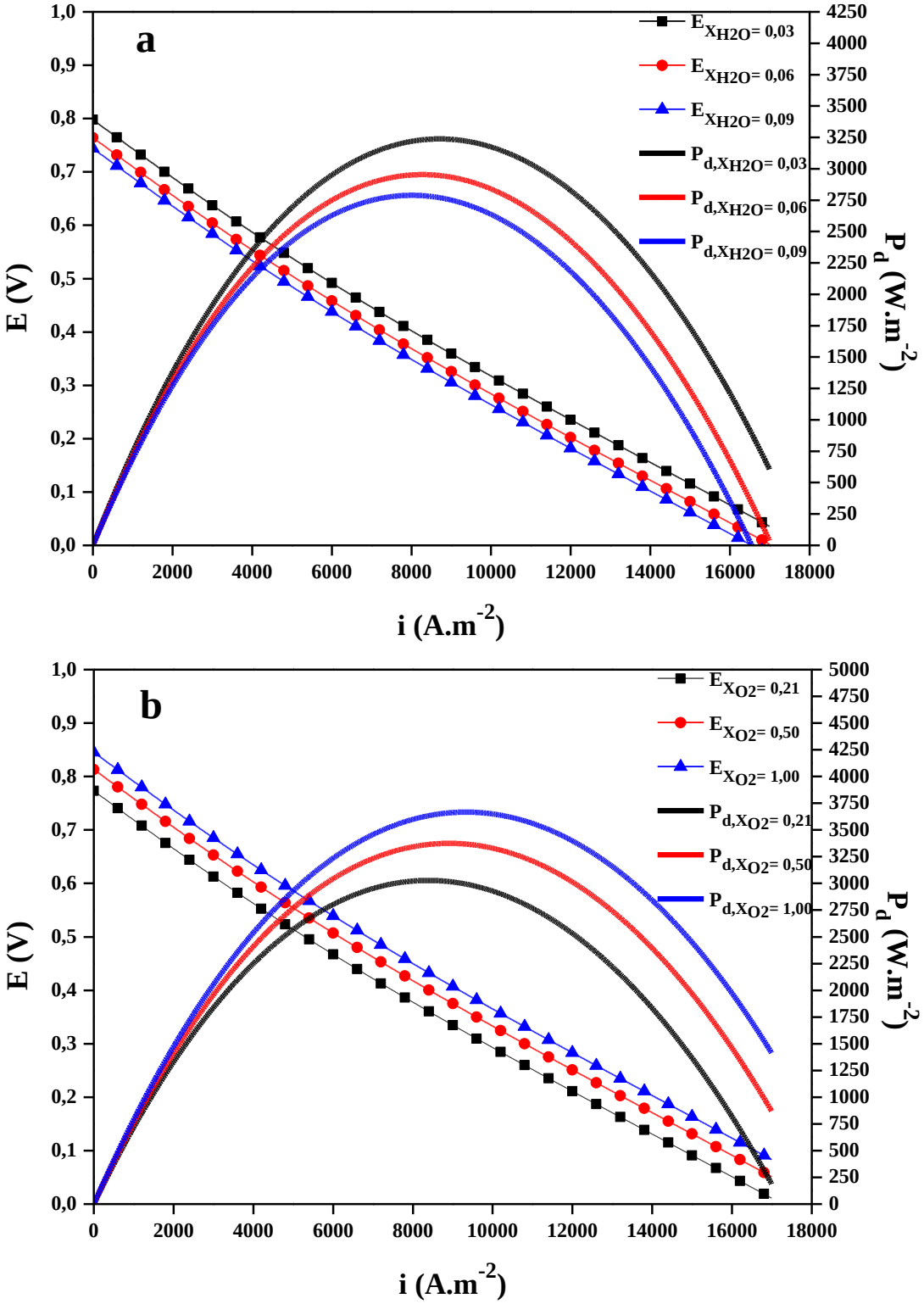

FIGURE 5. Potential and power density evolution according to the H_2O and O_2 concentration. a) H_2O concentration effect, b) O_2 concentration effect.

3.5. Electrolyte Thickness Effect

The electrolyte thickness effect on the polarization and power density curves is shown in Figure 6. The fuel is a humidified hydrogen (X_{H2O} = 0,05) and the oxidant is the air (X_{O2} = 0,21). Supply pressure values are common for the fuel and air (1 bar). The operating temperature is equal to (1073 K). Electrolyte thicknesses are taken equivalent to (5, 50 and 500 µm). The obtained values of the ideal and Nernst potentials in all the realized tests according to several electrolyte thicknesses are the same, which demonstrates that the electrolyte dimensions do not affect the Nernst and ideal potentials. Highest values of the real potential and the power density are obtained in the case of the smallest electrolyte thickness. However, the lowest values of the real potential and the power density are identical to the produced values by the cell having the largest electrolyte thickness. Logically, the real potential and power density values corresponding to a medium electrolyte thickness are between the values of the two real potentials and the two power densities presented by the two electrolyte dimensions mentioned earlier. It confirms that the real potential and the power density are inversely proportional to the electrolyte thickness.

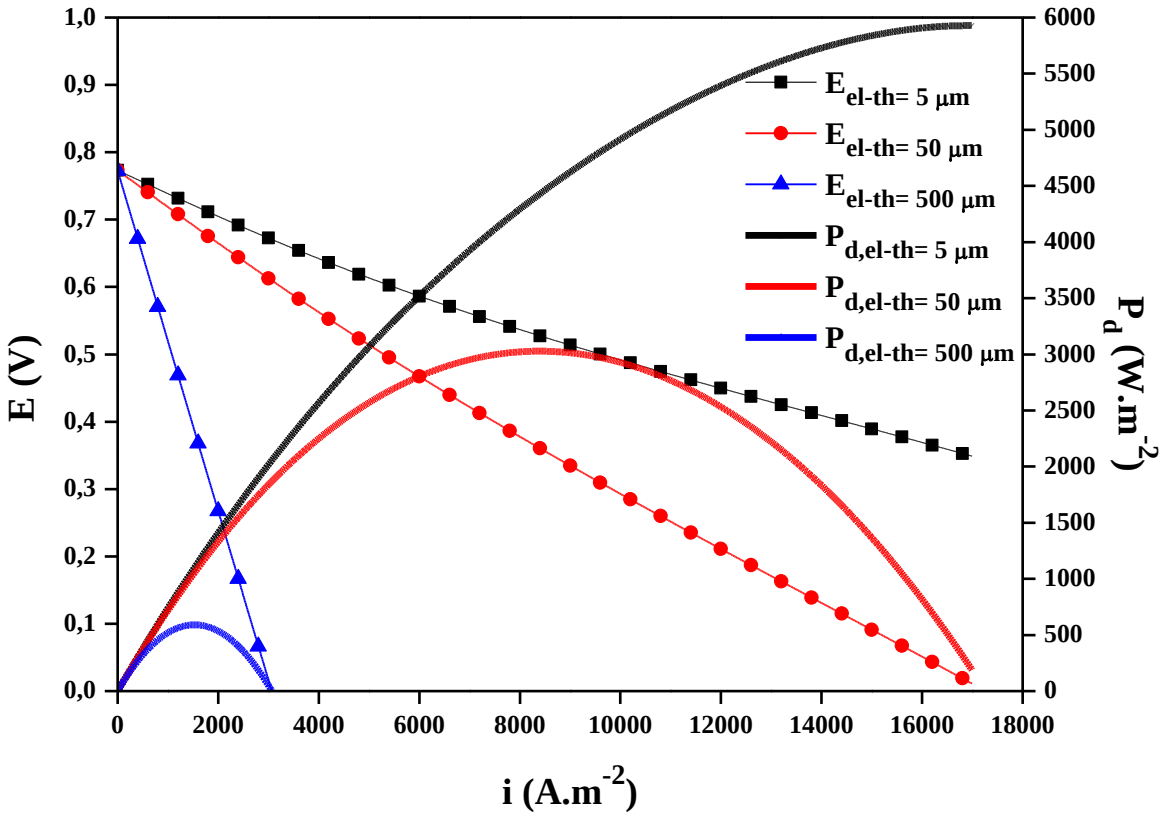

FIGURE 6. Potential and power density evolution according to electrolyte thickness.

4. Conclusions

SOFC is an electrochemical device. It serves to convert the chemical energy to the electrical and thermal energies. This study is based on the SOFC thermodynamic performance study. Particular attention is given to the delivered power density optimization. Mathematical equations are solved using a program in the FORTRAN language that is developed locally. Based on the obtained result analysis, it appeared that the developed model by combining the several sub-models can be a design tool. The main results are:

- The greatest loss is only generated by the Ohmic polarization. The smallest produced loss is due to the reactant diffusion in the catalytic sites. It can be neglected compared to the activation and Ohmic losses.

- SOFC potential and power density are proportional to the operating temperature and to the oxidant oxygen concentration.

- The potential and the power density are inversely proportional to the supply pressure, to the fuel humidification and to the electrolyte thickness.

References

[1] S. Yang, T. Chen, Y. Wang, Z. Peng, W.G. Wang, Electrochemical Analysis of an Anode-Supported SOFC, International Journal of Electrochemical Science, **8**(2), (2013), 2330-2344.

[2] A. AlZahrani, I. Dincer, X. Li, A performance assessment study on solid oxide fuel cells for reduced operating temperatures, International Journal of Hydrogen Energy, **40**(24), (2015), 7791-7797.

[3] J.K. Verma, A. Verma, A.K. Ghoshal, Performance analysis of solid oxide fuel cell using reformed fuel, International Journal of Hydrogen Energy, **38**(22), (2013), 9511-9518.

[4] D. Saebea, S. Authayanun, Y. Patcharavorachot, W. Paengjuntuek, A. Arpornwichanop, Use of different renewable fuels in a steam reformer integrated into a solid oxide fuel cell: Theoretical analysis and performance comparison, Energy, **51**(1), (2013), 305-313.

[5] P. Tippawan, A. Arpornwichanop, Energy and exergy analysis of an ethanol reforming process for solid oxide fuel cell applications, Bioresource Technology, **157**(1), (2014), 231-239.

[6] B. Zitouni, H. Ben Moussa, K. Oulmi, Studying on the increasing temperature in IT-SOFC: Effect of heat sources, Journal of Zhejiang University SCIENCE A, **8**(09), (2007), 1500-1504.

[7] B. Zitouni, H. Ben Moussa, K. Oulmi, S. Saighi, K. Chetehouna, Temperature field, H_2 and H_2O mass transfer in SOFC single cell: Electrode and electrolyte thickness effects, International Journal of Hydrogen Energy, **34**(11), (2009), 5032-5039.

[8] B. Zitouni, G.M. Andreadis, H. Ben Moussa, H. Abdenebi, D. Haddad, M. Zeroual, Two-dimensional numerical study of temperature field in an anode supported planar SOFC: Effect of the chemical reaction, International Journal of Hydrogen Energy, **36**(6), (2011), 4228-4235.

[9] K. Oulmi, B. Zitouni, H. Ben Moussa, H. Abdenebi, G.M. Andreadis, Total polarization effect on the location of maximum temperature value in planar SOFC, International Journal of Hydrogen Energy, **36**(6), (2011), 4236-4243.

[10] H. Abdenebi, B. Zitouni, D. Haddad, H. Ben Moussa, M.A. George, S. Abdessemed, SOFC fuel cell heat production: Analysis, Energy Procedia **6**(1), (2011), 643-650.

[11] H. Ben Moussa, B. Zitouni, K. Oulmi, B. Mahmah, M. Belhamel, P. Mandin, Hydrogen consumption and power density in a co-flow planar SOFC, International Journal of Hydrogen Energy, **34**(11), (2009), 5022-5031.

[12] D. Haddad, H. Abdenebi, B. Zitouni, H. Ben Moussa, K. Oulmi, Thermal field in SOFC fed by hydrogen: Inlet gases temperature effect, International Journal of Hydrogen Energy, **38**(20), (2013), 8575-8583.

[13] H. Abdenebi, B. Zitouni, H. Ben Moussa, D. Haddad, Thermal field in SOFC fed by CH4: Molar fractions effect, Journal of the Association of Arab Universities for Basic and Applied Sciences, **17**(1), (2015), 82-89.

[14] H. Abdenebi, B. Zitouni, H. Ben Moussa, D. Haddad, H. Zitouni, Y. Sahli, Inlet Methane Temperature Effect at a Planar SOFC Thermal Field Under Direct Internal Reforming Condition, In I. Dincer, C. Ozgur Colpan, O. Kizilkan and M. Akif Ezan

(eds), Progress in clean energy volume II: Novel Systems and Applications, Switzerland: Springer, 567-581 (2015).

[15] Y. Sahli, B. Zitouni, H. Ben Moussa, H. Abdenebi, Three-Dimensional Numerical Study of the Heat Transfer on the Planar Solid Oxide Fuel Cell: Joule's Effect, In I. Dincer, C. Ozgur Colpan, O. Kizilkan and M. Akif Ezan (eds), Progress in clean energy volume I: Analysis and Modeling, Switzerland: Springer, 449-461 (2015).

[16] A. Arpornwichanop, Y. Patcharavorachot, S. Assabumrungrat, Analysis of a proton-conducting SOFC with direct internal reforming, Chemical Engineering Science, **65**(1), (2010), 581-589.

[17] Y. Patcharavorachot, N.P. Brandon, W. Paengjuntuek, S. Assabumrungrat, A. Arpornwichanop, Analysis of planar solid oxide fuel cells based on proton-conducting electrolyte, Solid State Ionics, **181**(35-36), (2010) 1568-1576.

[18] Y. Patcharavorachot, W. Paengjuntuek, S. Assabumrungrat, A. Arpornwichanop, Performance evaluation of combined solid oxide fuel cells with different electrolytes, International Journal of Hydrogen Energy, **35**(9), (2010), 4301-4310.

[19] M. Ni, An electrochemical model for syngas production by co-electrolysis of H_2O and CO_2, Journal of Power Sources, **202**(1), (2012), 209-216.

[20] R.K. Akikur, R. Saidur, H.W. Ping, K.R. Ullah, Performance analysis of a co-generation system using solar energy and SOFC technology, Energy Conversion and Management, **79**(1), (2014), 415-430.

[21] M. Andersson, H. Nakajima, T. Kitahara, A. Shimizu, T. Koshiyama, H. Paradis, J. Yuan, B. Sundén, Comparison of humidified hydrogen and partly pre-reformed natural gas as fuel for solid oxide fuel cells applying computational fluid dynamics, International Journal of Heat and Mass Transfer, **77**(1), (2014), 1008-1022.

[22] B.H. Choi, H.J. Sung, Effect of a shielded slot on a planar solid oxide fuel cell, International Journal of Hydrogen Energy, **39**(24), (2014), 12913-12923.

[23] M. Saidi, F. Siavashi, M.R. Rahimpour, Application of solid oxide fuel cell for flare gas recovery as a new approach: a case study for Asalouyeh gas processing plant, Iran, Journal of Natural Gas Science & Engineering, **17**(1), (2014), 13-25.

[24] K. Zheng, L. Li, M. Ni, Investigation of the electrochemical active thickness of solid oxide fuel cell anode, International Journal of Hydrogen Energy, **39**(24), (2014), 12904-12912.

[25] J.R. Ferguson, J.M. Fiard, R. Herbin, Three-dimensional numerical simulation for various geometries of solid oxide fuel cells, Journal of Power Sources, **58**(1), (1996), 109-122.

[26] M.M. Hussain, X. Li, I. Dincer, Mathematical modeling of planar solid oxide fuel cells, Journal of Power Sources, **161**(1), (2006), 1012-1022.

[27] L. Andreassi, G. Rubeo, S. Ubertini, P. Lunghi, R. Bove, Experimental and numerical analysis of a radial flow solid oxide fuel cell, International Journal of Hydrogen Energy, **32**(17), (2007), 4559-4574.

[28] X. Zhang, G. Li, J. Li, Z. Feng, Numerical study on electric characteristics of solid oxide fuel cells, Energy Conversion and Management, **48**(1), (2007), 977-989.

[29] C. Bao, N. Cai, E. Croiset, A multi-level simulation platform of natural gas internal reforming solid oxide fuel cell-gas turbine hybrid generation system-Part II. Balancing units model library and system simulation, Journal of Power Sources, **196**(1), (2011), 8424-8434.

[30] M. Andersson, H. Paradis, J. Yuan, B. Sundén, Three dimensional modeling of an solid oxide fuel cell coupling charge transfer phenomena with transport processes and heat generation, Electrochimica Acta, **109**(1), (2013), 981-993.

[31] M. Andersson, J. Yuan, B. Sundén, SOFC modeling considering hydrogen and carbon monoxide as electrochemical reactants, Journal of Power Sources, **232**(1), (2013), 42-54.

[32] D. Saebea, Y. Patcharavorachot, S. Assabumrungrat, A. Arpornwichanop, Analysis of a pressurized solid oxide fuel cell-gas turbine hybrid power system with cathode gas recirculation, International Journal of Hydrogen Energy, **38**(11), (2013), 4748-4759.

[33] X. Zhang, S. Su, J. Chen, Y. Zhao, N. Brandon, A new analytical approach to evaluate and optimize the performance of an irreversible solid oxide fuel cell-gas turbine hybrid system, International Journal of Hydrogen Energy, **36**(23), (2011), 15304-15312.

[34] X. Zhang, Y. Wang, J. Guo, T. Shih, J. Chen, A unified model of high-temperature fuel-cell heat-engine hybrid systems and analyses of its optimum performances, International Journal of Hydrogen Energy, **39**(4), (2014), 1811-1825.